Journal of Power Sources 270 (2014) 468–474

Contents lists available at ScienceDirect

Journal of Power Sources

journal homepage: www.elsevier.com/locate/jpowsour

Silver-incorporated composites of Fe_2O_3 carbon nanofibers as anodes for high-performance lithium batteries

Mingzhong Zou [a], Jiaxin Li [a, b], WeiWei Wen [a], Luzhuo Chen [a], Lunhui Guan [b], Heng Lai [a, *], Zhigao Huang [a, *]

[a] College of Physics and Energy, Fujian Normal University, Fujian Provincial Key Laboratory of Quantum Manipulation and New Energy Materials, Fuzhou 350007, China
[b] Fujian Institute of Research on the Structure of Matter, Chinese Academy of Sciences, Fuzhou 350002, China

HIGHLIGHTS

- Ag–Fe_2O_3/CNF anode materials were synthesized by a facile electrospinning process.
- The Ag–Fe_2O_3/CNFs exhibit high capacity, excellent cyclic stability and good rate performance for lithium ion batteries.
- The enhanced performance is ascribed to the synergetic effects between Ag doping and carbon supports of CNFs.

GRAPHICAL ABSTRACT

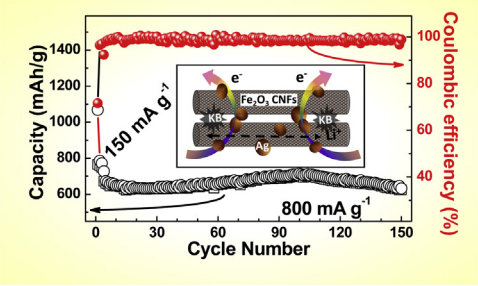

ARTICLE INFO

Article history:
Received 19 May 2014
Received in revised form
1 July 2014
Accepted 18 July 2014
Available online 30 July 2014

Keywords:
Silver-incorporated carbon nanofibers
Fe_2O_3 anode
Electrochemical performance
Impedance analysis
Electrospinning method

ABSTRACT

Composites of Ag-incorporated carbon nanofibers (CNFs) confined with Fe_2O_3 nanoparticles (Ag–Fe_2O_3/CNFs) have been synthesized through an electrospinning method and evaluated as anodes for lithium batteries (LIBs). The obtained Ag–Fe_2O_3/CNF anodes show good LIB performance with a capacity of 630 mAh g^{-1} tested at 800 mA g^{-1} after 150 cycles with almost no capacity loss and superb rate performance. The obtained properties for Ag–Fe_2O_3/CNF anodes are much better than Fe_2O_3/CNF anodes without Ag-incorporating. In addition, the low-temperature LIB performances for Ag–Fe_2O_3/CNF anodes have been investigated for revealing the enhanced mechanism of Ag-incorporating. The superior electrochemical performances of the Ag–Fe_2O_3/CNFs are associated with a synergistic effect of the CNF matrix and the highly conducting Ag incorporating. This unique configuration not only facilitates electron conduction especially at a relative temperature, but also maintains the structural integrity of active materials. Meanwhile, the related analysis of the AC impedance spectroscopy and the corresponding hypothesis for DC impedance confirm that such configuration can effectively enhance the charge-transfer efficiency and the lithium diffusion coefficient. Therefore, CNF-supported coupled with Ag incorporating synthesis supplied a promising route to obtain Fe_2O_3 based anodes with high-performance LIBs especially at low temperature.

1. Introduction

Recently, lithium batteries (LIBs) have attached much attention because of their high energy density and power density, which could be widely applied in hybrid vehicles and energy sources

* Corresponding authors. Tel./fax: +86 591 22867577.
E-mail addresses: ljx@fjirsm.ac.cn (J. Li), laiheng@fjnu.edu.cn (H. Lai), zghuang@fjnu.edu.cn (Z. Huang).

http://dx.doi.org/10.1016/j.jpowsour.2014.07.119
0378-7753/

[1–10]. However, owing to the low theoretical capacity of 372 mAh g^{-1}, graphite cannot meet the requirements of new emerging technologies [8,9]. Thus, major challenges of the next-generation LIBs have demanded development of alternative anode materials with high energy density, long cycle life, and high rate capability.

Several metal oxides, especially for Fe_2O_3 materials with high theoretical capacities of 1007 mAh g^{-1}, low cost and environmental friendliness, have been widely investigated as promising anode materials for high energy density LIBs [4–10]. However, Fe_2O_3 materials often suffer from rapid capacity fading arising from kinetic limitation, agglomeration and volume expansion during the cycling process [11]. To improve their LIB performance, two basic strategies have been developed. One is to design Fe_2O_3 with different nanostructures such as nanorods [12], nanoflakes [13] and nanocapsules [14]. The other is to use carbonaceous materials as buffer carriers for Fe_2O_3-based composites [15–18]. These carbonaceous materials, including carbon nanofibers (CNFs) [15], carbon nanotubes [16,17] and grapheme [18], could not only improve the conductivity of Fe_2O_3 composite, but also effectively suppress the large volume expansion of Fe_2O_3 during discharge and charge cycles, further improving the electrochemical performances of Fe_2O_3 composites. Herein, CNFs with unique structure, large aspect ratio, high conductivity, and favorable flexibility have been proven to be good candidates. For example, *Wu* et al. [15] synthesized a porous Fe_2O_3 NP@CNF composite, which delivered a capacity of 830 mAh g^{-1} after 40 cycles at a current density of 50 mA g^{-1}. *Zhang* et al. [19] prepared CNFs with Fe_2O_3 nanoparticles through a simple electrospinning process. The obtained composites showed superior cyclability for 100 cycles with a reversible capacity of 820 mAh g^{-1} at a current density of 0.2C. Anyhow, to further develop composites of Fe_2O_3 combined with CNF buffer carrier with better performance is still needed.

In addition, exploring alternative anodic materials with high-performance especially at low temperature has become another urgent task today [20–25]. Typically for composites of Fe_2O_3 combined with CNF buffer carrier, Fe_2O_3 as a kind of semiconductor would present an increasing electric resistance with decreasing temperature. Meanwhile, the reduced ability of carbonaceous materials to intercalate lithium into their structures at low temperatures would be also deteriorated, which may be attributed to the high charge-transfer resistance. To some extent, improving the conductivity of electrode can alleviate the related problems. According to the previous reports [24,25], graphite mixed with metals nanoparticles dispersed in the carbon matrix, and graphite electrodes covered with a metal layer have shown improvements in the electrochemical behavior at low temperatures. Thus, how to use an effective method to simultaneously design and fabricate composites of Fe_2O_3 combined with CNF for highly energy LIBs is highly desired, especially at low temperature.

In this study, Ag-incorporated CNFs confined Fe_2O_3 (Ag–Fe_2O_3/CNFs) anode have been prepared by electrospinning and evaluated as anodes for LIBs. These anodes provided with the unique architectures exhibit outstanding lithium battery performances both in the room temperature and the low temperature of −5 °C. Moreover, the mechanism for the enhanced LIB performance resulting from the CNF carrier and Ag-incorporating was investigated by electrochemical impedance spectroscopy.

2. Experimental section

2.1. Materials synthesis

All chemicals in experiment were of analytical grade and used as received. Typically, 1.0 g of polyvinylprrolidone (PVP, M_w, 130000) was dissolved in 12 ml of ethyl alcohol and deionized water, and then 0.97 g of $AgNO_3$ and 14.0 g of $Fe(NO_3)_3 \cdot 9H_2O$ were added to form a mixed solution. After vigorous stirring for 40 h at 60 °C, a sticky sol was obtained. For comparison, 24 ml of ethyl alcohol and deionized water containing 2.0 g PVP and 14.0 g of $Fe(NO_3)_3 \cdot 9H_2O$ ware also prepared without adding $AgNO_3$. Furthermore, the pure Ag-CNFs were prepared under the same condition above-mentioned without adding $Fe(NO_3)_3 \cdot 9H_2O$. According to our previous work [26], a 20 kV high voltage was used for electrospinning. The speed rate and distance were set up at 0.6 ml h^{-1} and 15 cm, respectively. The PVP nanofibers were collected on a rounded collector, and then dried for 24 h in vacuum at 80 °C. The dried nanofibers were further stabilized in air at 240 °C for 4 h with a heating rate of 2 °C min^{-1}. Finally, the stabilized nanofibers were annealed in Ar atmosphere flow at 430 °C for 1 h with a heating rate of 2 °C min^{-1} for forming Ag-incorporated carbon nanofibers confined with Fe_2O_3 nanoparticles.

2.2. Materials characterization

These samples were characterized by X-ray diffraction (XRD, RIGAKU SCXmini), X-ray photoelectron spectroscopy (XPS, VG Scientific ESCALAB MK II), scanning electron microscope (SEM, JSM-6700F), transmission electron microscope (TEM, Tecnai G2 F20) and thermogravimetry analyses (TGA, NETZSCH STA449C).

2.3. Electrochemical measurements

The electrochemical behaviors were measured via CR2025 coin-type cells assembled in a dry argon-filled glove box. The test cell consisted of working electrode (about ~1.5 mg cm^{-2}) and lithium sheet which were separated by a Celgard 2300 membrane and electrolyte of 1 M $LiPF_6$ in EC:EMC:DMC (1:1:1 in volume). The working electrode consisted of 80 *wt.* % active material, 10 *wt.* % acetylene black, and 10 *wt.* % polymer binders (Carboxymethyl cellulose, Na-CMC). These electrochemical properties are all calculated based on the overall mass of the active material of Fe_2O_3/CNFs or Ag–Fe_2O_3/CNFs. The cells were cycled by LAND2001A at room temperature. Cyclic voltammetry curves (CVs) were tested on a CHI660D Electrochemical Workstation. Electrochemical impedance measurements were carried out by applying an ac voltage of 5 mV over the frequency range from 1 mHz to 100 kHz.

3. Result and discussion

The crystalline structure of the Fe_2O_3/CNFs and Ag–Fe_2O_3/CNFs were investigated by XRD. From Fig. 1, the diffraction peaks at 30.2°,

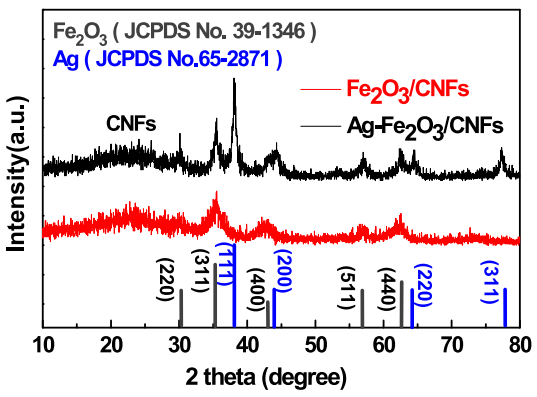

Fig. 1. XRD pattern of the Ag–Fe_2O_3/CNFs and Fe_2O_3/CNFs.

35.6°, 43.3°, 57.3° and 62.9° presented both in Fe_2O_3/CNFs and Ag–Fe_2O_3/CNFs can be well-assigned to the (220), (311), (400), (511) and (440) planes of Fe_2O_3 crystal according to the standard data file (JCPDS no. 39-1346). The diffraction peak of CNFs near 26.5° can be observed in both of composites. Compared with the Fe_2O_3/CNFs, Ag–Fe_2O_3/CNFs present four additional clear diffraction peaks located at 38.1°, 44.3°, 64.4° and 77.5°, which are matched well with the (111), (200), (220) and (311) crystal planes of Ag (JCPDS no. 65-2871). Thus, it is suggested that Ag was successfully introduced into the composite, thus providing a good conductivity for the Ag-incorporated Fe_2O_3/CNF composite. In addition, the weak and broad peaks for Fe_2O_3 indicate their nano-crystalline particles. Meanwhile, a slightly sharp peak of Ag (111) reveals that there exhibits the good crystalline for Ag. These findings are in agreement with the following TEM results.

As shown in Fig. 2, the morphologies and structure of the Ag–Fe_2O_3/CNFs were examined by SEM, EDS, TEM and HR-TEM. From Fig. 2(a), SEM image reveals that Ag–Fe_2O_3/CNFs are consisted of randomly oriented, overlapped, continuous and interconnected nanofibers. The diameter for these nanofibers is ranging from 250 to 550 nm. It should be also noted that the CNFs are attached with some relatively uniform particles, which should be identified as Ag particles. The same results can also be found in the TEM related results shown in Fig. 2. The TEM, HR-TEM and the corresponding SAED analysis of Ag–Fe_2O_3/CNFs are shown in Fig. 2(b–d), respectively. The presence of Ag particles with dark shadow morphology ranged from 5 to 35 nm can be clearly observed in Fig. 2(b) and Fig. S1 (shown in ESI). The HR-TEM image shown in Fig. 2(c) reveals the interplanar spacing of 0.29 and 0.25 nm, corresponding to the (220) and (311) planes of Fe_2O_3 in Ag–Fe_2O_3/CNFs. The diffraction rings from the selected area electron diffraction (SAED) pattern (Fig. 2(d)) also confirm the formation of crystalline Fe_2O_3 and Ag in the CNFs. In addition, the EDS and element mapping (Fig. 2(e–j)) provide another proof of Ag incorporating in the CNFs. As presented in Fig. 2(g–i), it can be seen that C, O and Fe are homogeneously distributed in the composite, indicating the Fe_2O_3 is homogenously distributed in the CNFs. Herein, Fig. 2(j) also reveals that some relatively uniform Ag particles attached on the CNFs. In other words, such structure observed from Fig. 2(a) makes these net-like Ag–Fe_2O_3/CNFs accessible for using as superior anode materials for LIBs.

In addition to the analysis for Ag–Fe_2O_3/CNFs, the morphology and structure of the pure Fe_2O_3/CNFs were also respectively examined by the SEM, EDS, TEM and HR-TEM shown in Figs. S2–3. Unlike Ag–Fe_2O_3/CNFs, SEM image for Fe_2O_3/CNFs shows interconnected nanofibers with smooth surface. Furthermore, TGA tests were measured from 30 to 800 °C at a heating rate of 10 K min^{-1} in air, to evaluate the weight content of Ag and Fe_2O_3 in these hybrid materials. Based on the TGA results in Figs. S4, S5 and Table S1, the loading ratio of Fe_2O_3 in Fe_2O_3/CNFs is 72 *wt*. %, and that of Ag and Fe_2O_3 in Ag–Fe_2O_3/CNFs are about 14 *wt*. % and 72 *wt*. %, respectively.

The cyclic voltammetry (CV) curves of Fe_2O_3/CNF and Ag–Fe_2O_3/CNF electrodes at the first 10 cycles in the voltage window of 3.0–0.05 V at scan rate of 0.5 mV s^{-1} are shown in Fig. 3(a) and (b). According to the previous report [27], the cathodic peak around 1.25 V in the 1st cycle shown in Fig. 3(a) corresponds to the reaction of Fe^{3+} to Fe^{2+}. The peak at 0.75 V with a sloping curve down to the cutoff voltage of 0.05 V is attributed to the reaction of Fe^{2+} to Fe^0 and the formation of the solid electrolyte interface (SEI) layer. The anodic peak presented from 1.5 V to 2.2 V represents the oxidation from Fe^0 to Fe^{3+}. In the subsequent 9 cycles, the 0.75 V reduction peak becomes diminished, indicating that formation of the SEI layer only takes place during the 1st cycle. Compared to the CV curves of

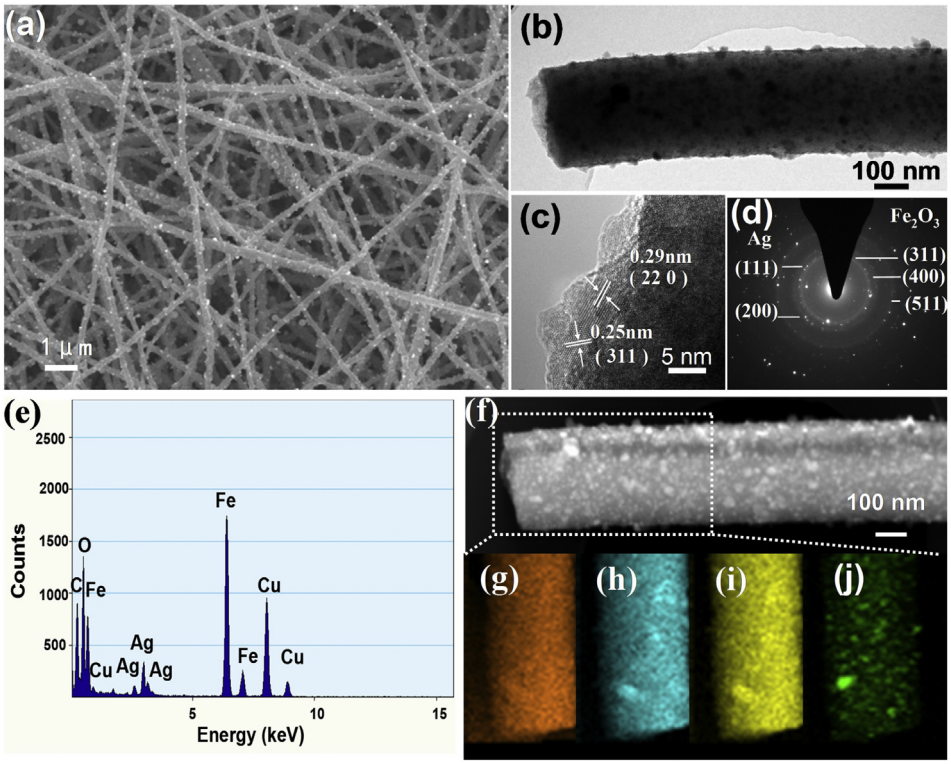

Fig. 2. (a) SEM images of the Ag–Fe_2O_3/CNFs; (b) TEM images of the Ag–Fe_2O_3/CNFs; (c) and (d) HR-TEM images and SAED pattern of the Ag–Fe_2O_3/CNFs; (e) EDX images of the Ag–Fe_2O_3/CNFs; (f) TEM images of the Ag–Fe_2O_3/CNFs; (g)–(j) element mappings of carbon (orange), iron (green), oxygen (yellow), and silver (green), respectively. (For interpretation of the references to color in this figure legend, the reader is referred to the web version of this article.)

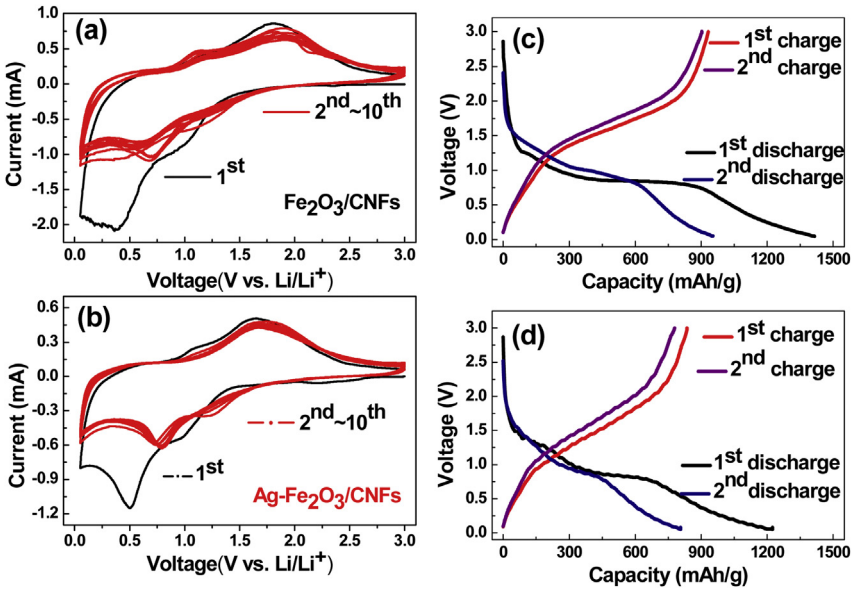

Fig. 3. Cyclic voltammetry curves and first two discharge–charge curves between 0.05 and 3 V of Li insertion/extraction into/from two electrodes: (a, c) Fe_2O_3/CNF electrode and (b, d) Ag–Fe_2O_3/CNF electrode.

Fe_2O_3/CNFs shown in Fig. 3(a), it is observed from Fig. 3(b) that the peaks in the following 9 cycles overlap well, indicating that a better electrochemical reversibility and structural stability for Ag–Fe_2O_3/CNFs. Accordingly, the discharge/charge (D/C) profiles of the Fe_2O_3/CNFs and Ag–Fe_2O_3/CNF electrodes in the first two cycles at a current density of 150 mA g^{-1} between 0.05 V and 3.00 V are presented in Fig. 3(c) and (d), respectively. Those voltage plateaus shown in D/C curves for the Fe_2O_3/CNF and Ag–Fe_2O_3/CNF electrodes are consistent with the CV observation. The D/C profiles show similar features to those of nano-sized Fe_2O_3 reported previously. The reaction mechanism of Li and Fe_2O_3 could be described as follows [27]:

$$Fe_2O_3 + 2Li^+ + 2e^- \rightarrow Li_2(Fe_2O_3) \quad (1)$$

$$Li_2(Fe_2O_3) + 4Li^+ + 4e^- \rightarrow 2Fe^0 + 3Li_2O \quad (2)$$

$$2Fe^0 + 2xLi_2O \leftrightarrow 2FeO_x + 4xLi^+ + 4xe^- \quad (3)$$

In addition, it is found from Fig. 3(c) that the first D/C curves of Fe_2O_3/CNF electrode deliver capacities of 1414 and 932 mAh g^{-1}, implying an irreversible capacity loss of ~34.1%. In contrast, the first D/C capacities for the Ag–Fe_2O_3/CNF electrode were 1223 and 835 mAh g^{-1}, with a smaller irreversible capacity loss of ~31.7% compared to that of Fe_2O_3/CNFs. On the other hand, the lower initial discharged capacity for Ag–Fe_2O_3/CNFs is obtained, which may be resulted from the additional weight of Ag element Ag–Fe_2O_3/CNFs.

The comparison of cycling performance for Fe_2O_3/CNF and Ag–Fe_2O_3/CNF electrodes at different current densities is shown in Fig. 4. Fig. 4(a) compares the cycling performances of these two anodes measured at 200 mA g^{-1}. Apparently, the Ag–Fe_2O_3/CNF electrode exhibits a significantly improved reversible capacity. After 70 cycles, the reversible capacity of Ag–Fe_2O_3/CNFs remained at 656 mAh g^{-1}, while that of only 500 mAh g^{-1} for the Fe_2O_3/CNFs. Meanwhile, the cycle performances of the Fe_2O_3/CNF and Ag–Fe_2O_3/CNF electrodes have been tested at a relatively high current densities of 600 mA g^{-1} after being activated at 150 mA g^{-1} in the first three cycles, as shown in Fig. 4(b). Similarly, the electrochemical performance for Ag–Fe_2O_3/CNF electrode is better than that of Fe_2O_3/CNF electrode. Furthermore, in order to investigate the excellent rate capability in detail, the result for these two electrodes discharged and charged at various rates is shown in Fig. 4(c). Both of these two electrodes show good capacity retentions at different rates. However, after 60 cycles, a large reversible capacity of 830 mAh g^{-1} remained for 10 cycles was resumed for Ag–Fe_2O_3/CNFs when the rate was reduced back to 200 mA g^{-1}, demonstrating a better high-rate performance than that of Fe_2O_3/CNF electrode. The composite of Ag–Fe_2O_3/CNFs with excellent cyclic stability as well as high rate performance, is comparable with the latest results on the Fe_2O_3 based anodes [15,17,19].

As shown in Fig. 5, the specific reversible capacity stabilized at 630 mAh g^{-1} even after 150 cycles, which capacity is much higher than the graphite of 372 mAh g^{-1}. Herein, subtracting the capacity contribution from Ag-CNFs in Ag–Fe_2O_3/CNFs, a reversible capacity of 782 mAh g^{-1} can be attributed to Fe_2O_3, indicating 78% of the theoretical capacity of Fe_2O_3 (1007 mAh g^{-1}). The capacity of 782 mAh g^{-1} and the ratio of 78% can be calculated by the following equations: $[C_{Ag\text{-}Fe2O3/CNFs} - (C_{Ag\text{-}NFs} * 26\ wt.\ \%)]/72\ wt.\ \% = [630 - (260 * 0.26)]/0.72 = 782$ and $782/1007 = 78\ \%$. Herein, the results of XRD, SEM, EDS and the corresponding electrochemical performance of Ag-CNFs are shown in the Figs. S6–10. Furthermore, by measuring at 200 mA g^{-1} (shown in Fig. 4(a)), the reversible capacity of Fe_2O_3 can almost achieve its theoretical capacity in this current study. The improved electrochemical performance for the Ag–Fe_2O_3/CNF composite can be attributed to the unique structure of the Ag incorporating CNFs, which may contribute positively to Li ion diffusion and Fe_2O_3 stabilization. According to the EIS result shown in Fig. 6 and Table S2, the good performance of Ag–Fe_2O_3/CNF composite is also ascribed to the good conductivity and electronic contact between Fe_2O_3 and Ag incorporating CNFs.

As we know, the charge-transfer resistance for carbonaceous materials would increase obviously with decreasing the temperature [24–25]. However, the case of metal Ag is contrast from that of carbonaceous materials. Thus, exploring those anodic materials of Ag–Fe_2O_3/CNFs especially at a low temperature is highly desired today. Here, Fig. 7 shows the electrochemical performances of these two anodes with a low temperature of −5 °C at different current densities of 200 mA g^{-1} and 600 mA g^{-1}. Interestingly, the reversible capacities for these two samples all maintain stable with

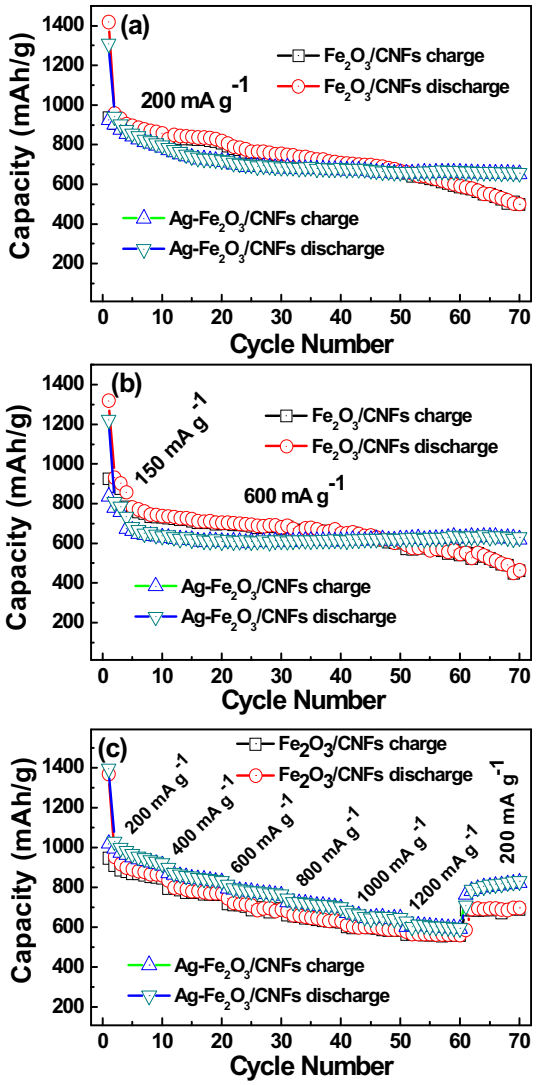

Fig. 4. Cycling performance of Fe_2O_3/CNF electrode and Ag–Fe_2O_3/CNF electrode at room temperature: (a) at a current density of 200 mA g^{-1}; (b) at a large current density of 600 mA g^{-1} and (c) at various current rates.

the increasing cycle number. However, after 65 cycles, the specific reversible capacity of 560 mAh g^{-1} at 600 mA g^{-1} for Ag–Fe_2O_3/CNFs are much larger than that of 260 mAh g^{-1} for Fe_2O_3/CNFs. Therefore, it is concluded that the Fe_2O_3/CNF composite with Ag

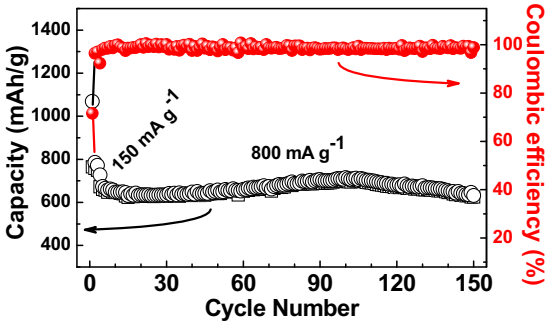

Fig. 5. Cycling performance of Ag–Fe_2O_3/CNF electrode at a large current density of 800 mA g^{-1} at room temperature.

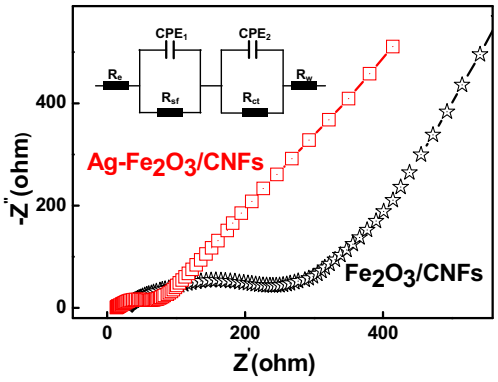

Fig. 6. Electrochemical impedance spectra for Fe_2O_3/CNF electrode and Ag–Fe_2O_3/CNF electrode after long electrochemical tested at room temperature.

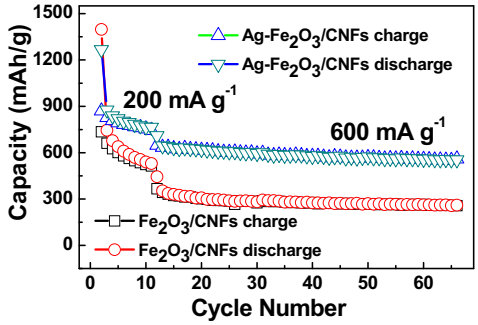

Fig. 7. Cycling performance of Fe_2O_3/CNF electrode and Ag–Fe_2O_3/CNF electrode at a current density of 600 mA g^{-1} at the low temperature of −5 °C.

incorporating can present an excellent electrochemical performance at a low temperature.

What is the possible reason for this result? Here, some insights about impedance analysis have been proposed for explaining the enhanced mechanism for LIBs. Fig. 8 shows EIS impedance spectra of Fe_2O_3/CNF and Ag–Fe_2O_3/CNF electrodes after long test at a low temperature and the corresponding equivalent circuit. According to the literature [28,29], the impedance spectra are fitted with an equivalent circuit as shown in the inset of Fig. 8. As is known, the SEI and charge-transfer-dominated regimes are reflected at high and intermediate frequencies, respectively, and in the range of low frequencies, diffusion of charge in anodes is the dominant factor. [28] The circuit consist of a bulk electrolyte resistance (R_e), a SEI

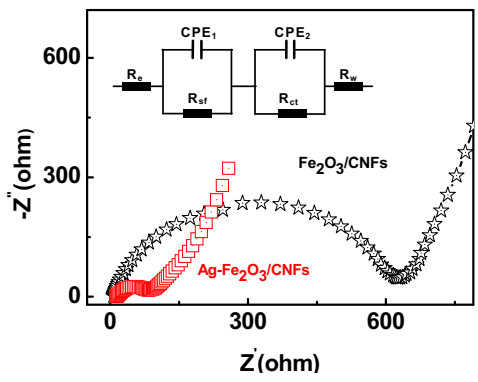

Fig. 8. Electrochemical impedance spectra for Fe_2O_3/CNF electrode and Ag–Fe_2O_3/CNF electrode after long electrochemical tested at the low temperature of −5 °C.

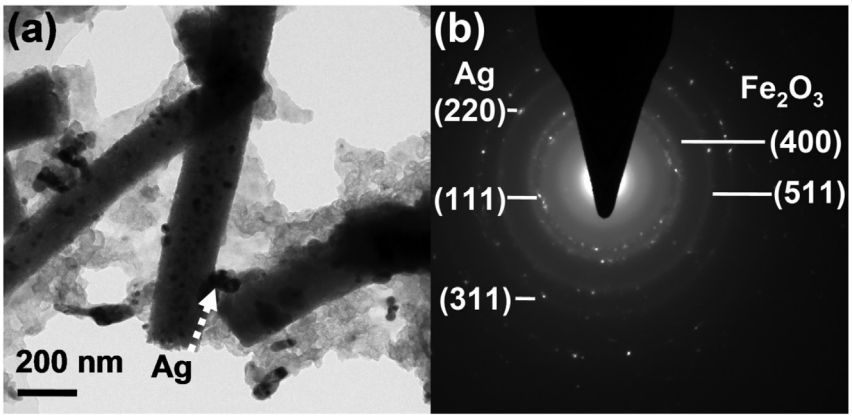

Fig. 9. TEM images and SAED pattern of the Ag–Fe_2O_3/CNFs after long electrochemical tested.

layer resistance (R_{SEI}), a charge transfer resistance (R_{ct}), two constant phase elements (CPE_1 and CPE_2), a semi-infinite Warburg impedance (R_w) describing the solid-state diffusion of Li^+ in low frequencies. As shown in Table S3, the fitting results of both samples indicate that the R_{sf} (84.3 Ω) and R_{ct} (21.5 Ω) values of Ag incorporating composite is much smaller than those of 631.6 Ω and 53.5 Ω for Fe_2O_3/CNFs, indicating that the presence of Ag incorporating can significantly improve the diffusion resistance and charge transfer resistance for electrodes.

To investigate the excellent electrochemical performance of Ag–Fe_2O_3/CNFs, we decomposed a cell after long-term cycling and analyzed the morphology of the anode by TEM and SAED. From Fig. 9, Ag particles were still attached on the Fe_2O_3/CNFs. Furthermore, the SAED result reveals that the crystalline structure for Ag–Fe_2O_3/CNFs can be remained. Other details about TEM images have been shown in Fig. S11. Thus, the good morphology retention after electrochemical testing shown in Fig. 9 can effectively facilitate the high stability of the Ag–Fe_2O_3/CNF composite. For possible practical application, the electrochemical mechanism under direct-current mode for these coin cells should be carried out. In addition, the degradation of the conductivity in electrode can result in an enhanced interface polarization, which is considered to be responsible for the deterioration of the electrochemical performance. According to our previous report [30], the phenomenological resistance model was set up and the corresponding DC equivalent circuit between active materials describing these processes is shown in Fig. 10 and Fig. S12, which includes the CNF resistance R_c, the Fe_2O_3 resistance R_{Fe2O3}, the Ag incorporating resistance R_{Ag}, and the R_e for surface resistance arising from the species on the anode surface, respectively. The total resistance of Ag–Fe_2O_3/CNFs in parallel is much smaller than the R_{Ag}. Similarly, the total resistance of Fe_2O_3/CNFs in parallel is much smaller than the R_C or R_e. Especially at a low temperature, the value difference of resistance between R_{Ag} and R_C (or R_e) would increase sharply. Thus, the presence of high electronic-conductive Ag in the composite is beneficial to reduce the total resistance, which further reduces the surface polarization for electrodes, especially at a low temperature. As a result, the electrochemical properties including cycling stability and rate performance can be improved with metal Ag incorporating. At least, this preliminary result manifests that composites of Ag–Fe_2O_3/CNFs are promising anode materials for good-performance lithium batteries.

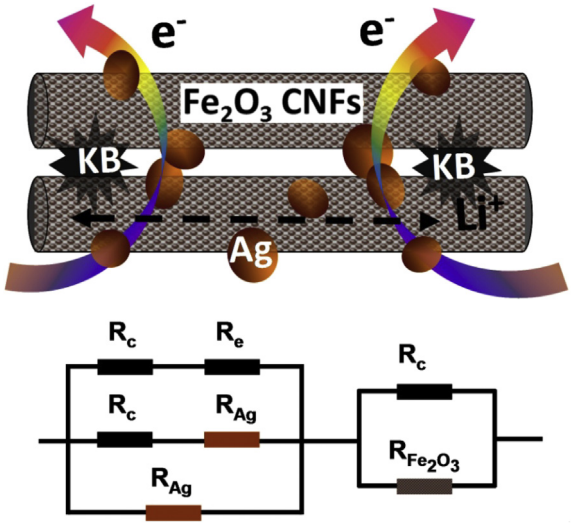

Fig. 10. The phenomenological resistance model and corresponding equivalent circuit for Ag–Fe_2O_3/CNFs.

4. Conclusion

In summary, composites of Ag-incorporated carbon nanofibers (CNFs) confined with Fe_2O_3 nanoparticles (Ag–Fe_2O_3/CNFs) have been synthesized through an electrospinning method and evaluated as anodes for lithium batteries (LIBs). Benefiting from the synergistic effect of the CNF matrix and the conducting Ag incorporating, the Ag–Fe_2O_3/CNF electrode displays high capacity, superior cyclic stability and excellent rate performance at both room temperature and low temperature (−5 °C). These preliminary results indicate the great potential application of CNF-supported coupled with Ag incorporating synthesis of metal oxide anodes for high-performance LIBs especially at low temperature.

Acknowledgment

We acknowledge the financial support by National Fundamental Research Program of China (Grant No. 2011CBA00200), the Natural Science Foundations of China (No. 21203025, No. 91127020, No. 51202031), Science and Technology Major Projects of Fujian Province (2013HZ0003) and Project of Fujian Development and Reform Commission (2013-577).

Appendix A. Supplementary data

Supplementary data related to this article can be found at http://dx.doi.org/10.1016/j.jpowsour.2014.07.119.

References

[1] M.V. Reddy, G.V. Subba Rao, B.V. Chowdari, Chem. Rev. 113 (2013) 5364–5457.
[2] L. Lu, X. Han, J. Li, J. Hua, M. Ouyang, J. Power Sources 226 (2013) 272–288.
[3] B. Scrosati, J. Hassoun, Y.-K. Sun, Energy Environ. Sci. 4 (2011) 3287.
[4] H. Lai, J. Li, Z. Chen, Z. Huang, ACS Appl. Mater. Interfaces 4 (2012) 2325–2328.
[5] K.W. Lim, J.I. Lee, J. Yang, Y.K. Kim, H.Y. Jeong, S. Park, H.S. Shin, ACS Appl. Mater. Interfaces 6 (2014) 6340.
[6] G. Fang, S. Kaneko, W. Liu, B. Xia, H. Sun, R. Zhang, J. Zheng, D. Li, Electrochim. Acta 111 (2013) 627–634.
[7] R. Thomas, G. Mohan Rao, Electrochim. Acta 125 (2014) 380–385.
[8] H. Kim, Y. Son, C. Park, J. Cho, H.C. Choi, Angew. Chem. 125 (2013) 6113–6117.
[9] J. Luo, J. Liu, Z. Zeng, C.F. Ng, L. Ma, H. Zhang, J. Lin, Z. Shen, H.J. Fan, Nano Lett. 13 (2013) 6136–6143.
[10] Y. Yang, X. Fan, G. Casillas, Z. Peng, G. Ruan, G. Wang, M.J. Yacaman, J.M. Tour, ACS Nano 8 (2014) 3939–3946.
[11] K.-A. Kwon, H.-S. Lim, Y.-K. Sun, K.-D. Suh, J. Phys. Chem. C 118 (2014) 2897–2907.
[12] L. Yu, Z. Wang, L. Zhang, H.B. Wu, X.W. Lou, J. Mater. Chem. A 1 (2013) 122.
[13] L. Li, H.B. Wu, L. Yu, S. Madhavi, X.W. Lou, Adv. Mater. Interfaces http://dx.doi.org/10.1002/admi.20140050
[14] S. Liu, R. Wang, M. Liu, J. Luo, X. Jin, J. Sun, L. Gao, J. Mater. Chem. A 2 (2014) 4598.
[15] Y. Wu, P. Zhu, M.V. Reddy, B.V. Chowdari, S. Ramakrishna, ACS Appl. Mater. Interfaces 6 (2014) 1951–1958.
[16] G. Zhou, D.-W. Wang, P.-X. Hou, W. Li, N. Li, C. Liu, F. Li, H.-M. Cheng, J. Mater. Chem. 22 (2012) 17942.
[17] M. Wu, J. Chen, C. Wang, F. Wang, B. Yi, W. Su, Z. Wei, S. Liu, Electrochim. Acta 132 (2014) 533.
[18] Y. Zou, J. Kan, Y. Wang, J. Phys. Chem. C 115 (2011) 20747–20753.
[19] X. Zhang, H. Liu, S. Petnikota, S. Ramakrishna, H.J. Fan, J. Mater. Chem. A 2 (2014) 10835.
[20] M. Marinaro, F. Nobili, A. Birrozzi, S.K. Eswara Moorthy, U. Kaiser, R. Tossici, R. Marassi, Electrochim. Acta 109 (2013) 207–213.
[21] M. Mancini, F. Nobili, S. Dsoke, F. D'Amico, R. Tossici, F. Croce, R. Marassi, J. Power Sources 190 (2009) 141–148.
[22] F. Nobili, S. Dsoke, M. Mancini, R. Tossici, R. Marassi, J. Power Sources 180 (2008) 845–851.
[23] F. Nobili, M. Mancini, S. Dsoke, R. Tossici, R. Marassi, J. Power Sources 195 (2010) 7090–7097.
[24] F. Nobili, S. Dsoke, T. Mecozzi, R. Marassi, Electrochim. Acta 51 (2005) 536–544.
[25] M. Marinaro, M. Pfanzelt, P. Kubiak, R. Marassi, M. Wohlfahrt-Mehrens, J. Power Sources 196 (2011) 9825–9829.
[26] J. Li, M. Zou, Y. Zhao, Z. Huang, L. Guan, RSC Adv. 3 (2013) 19251.
[27] J. Li, Y. Zhao, Y. Ding, L. Guan, RSC Adv. 2 (2012) 4205.
[28] S.-D. Xu, Q.-C. Zhuang, L.-L. Tian, Y.-P. Qin, L. Fang, S.-G. Sun, J. Phys. Chem. C 115 (2011) 9210–9219.
[29] C.-J. Cui, G.-M. Wu, H.-Y. Yang, S.-F. She, J. Shen, B. Zhou, Z.-H. Zhang, Electrochim. Acta 55 (2010) 8870–8875.
[30] J. Li, M. Zou, Y. Zhao, Y. Lin, H. Lai, L. Guan, Z. Huang, Electrochim. Acta 111 (2013) 165–171.